

# Detecting flavor content of the vacuum using the Dirac operator spectrum



Jian Liang,<sup>1,2,3,\*</sup> Andrei Alexandru,<sup>4</sup> Yu-Jiang Bi,<sup>5</sup> Terrence Draper,<sup>3</sup> Keh-Fei Liu,<sup>3</sup> and Yi-Bo Yang<sup>6,7,8,†</sup>  
( $\chi$ QCD Collaboration)

<sup>1</sup>Guangdong Provincial Key Laboratory of Nuclear Science, Institute of Quantum Matter,  
South China Normal University, Guangzhou 510006, China

<sup>2</sup>Guangdong-Hong Kong Joint Laboratory of Quantum Matter,  
Southern Nuclear Science Computing Center, South China Normal University, Guangzhou 510006, China

<sup>3</sup>Department of Physics and Astronomy, University of Kentucky, Lexington, KY 40506, USA

<sup>4</sup>Department of Physics, The George Washington University, Washington, DC 20052, USA

<sup>5</sup>Institute of High Energy Physics, Chinese Academy of Sciences, Beijing 100049, China

<sup>6</sup>CAS Key Laboratory of Theoretical Physics, Institute of Theoretical Physics, Chinese Academy of Sciences, Beijing 100190, China

<sup>7</sup>School of Fundamental Physics and Mathematical Sciences, Hangzhou Institute for Advanced Study, UCAS, Hangzhou 310024, China

<sup>8</sup>International Centre for Theoretical Physics Asia-Pacific, Beijing/Hangzhou, China

We compute the overlap Dirac spectrum on three ensembles generated using 2+1 flavor domain wall fermions. The spectral density is determined up to  $\lambda \sim 100$  MeV with sub-percentage statistical uncertainty. The three ensembles have different lattice spacings and two of them have quark masses tuned to the physical point. We show that we can resolve the flavor content of the sea quarks and constrain their masses using the Dirac spectral density. We find that the density is close to a constant below  $\lambda \leq 20$  MeV (but 10% higher than that in the 2-flavor chiral limit) as predicted by chiral perturbative theory ( $\chi$ PT), and then increases linearly due to the strange quark mass. Using the next to leading order  $\chi$ PT, one can extract the light and strange quark masses with  $\sim 20\%$  uncertainties. Using the non-perturbative RI/MOM renormalization, we obtain the chiral condensates at  $\overline{\text{MS}}$  2 GeV as  $\Sigma = (260.3(0.7)(1.3)(0.7)(0.8) \text{ MeV})^3$  in the  $N_f = 2$  (keeping the strange quark mass at the physical point) chiral limit and  $\Sigma_0 = (232.6(0.9)(1.2)(0.7)(0.8) \text{ MeV})^3$  in the  $N_f = 3$  chiral limit, where the four uncertainties come from the statistical fluctuation, renormalization constant, continuum extrapolation and lattice spacing determination. Note that  $\Sigma/\Sigma_0 = 1.40(2)(2)$  is much larger than 1 due to the strange quark mass effect.

*Introduction:* The QCD vacuum includes both quark and gluon. A gluon interacts with itself directly, but a quark can only interact with other quarks indirectly through a gluon. So a fundamental issue is how a quark's properties depend upon the flavors of virtual quarks in the vacuum.

The quark Dirac operator  $\mathcal{D} = (\partial_\mu - igA_\mu)\gamma_\mu$  is an efficient tool to address this question, as the quark flavors in the QCD vacuum (the “sea” quarks) just affect  $\mathcal{D}$  through the gluon field  $A_\mu$ . Based on the Banks-Casher relation [1], the near-zero density  $\rho(\lambda)$  of  $\mathcal{D}$  is proportional to the vacuum chiral condensate  $\langle \bar{\psi}\psi \rangle$ , which is the order parameter of spontaneous chiral symmetry breaking. By treating  $\lambda$  as an imaginary quark mass [2], chiral perturbative theory ( $\chi$ PT) reproduces the Banks-Casher relation as its leading order approximation, and provides a quantitative guide on the next-to-leading order (NLO) correction of  $\rho(\lambda)$  from the masses of different quark flavors in the vacuum, in the small quark mass region where  $\chi$ PT is still valid. But such a  $\chi$ PT calculation becomes quite complicated beyond the NLO region when the finite volume effects are taken into account, and its pre-

dictability is limited as there are many parameters in next-to-next leading order (NNLO).

On the other hand, nonperturbative lattice QCD can provide first-principles information about  $\rho(\lambda)$  which has been shown to be renormalizable [3, 4], while it is challenging to be precise and accurate enough to provide the flavor information of the vacuum. First of all, one must use the overlap fermion [5] or the projected Domain-wall fermion [6] to obtain  $\rho(\lambda)$  accurately at  $\lambda \sim 0$  [7–9], but at the expense of  $\mathcal{O}(10)$  or more computer time than that of the standard Wilson-like discretization of  $\mathcal{D}$  which breaks chiral symmetry explicitly. At the same time, one needs to solve the smallest eigenpairs (eigenvalue and corresponding eigenvector) of  $\mathcal{D}$ , count  $n(\lambda)$  and extract  $\rho(\lambda)$  accurately. This is  $\mathcal{O}(100)$  more expensive than the cost of a standard quark propagator. Thus the stochastic method has been proposed to provide some estimates of  $\rho(\lambda)$  [9–12].

During investigations in the last decade, the near-zero  $\mathcal{D}$  eigenpairs have been found to be extremely beneficial in lattice QCD calculations of the correlators to improve the signal-to-noise ratio using low-mode substitution (LMS) for the noise grid source [13–15]. These low modes tend to saturate the long-range parts of hadron correlators and are useful in calculating quark loops with the noise estimator needed only for the high modes [16].

\* jianliang@scnu.edu.cn

† ybyang@itp.ac.cn

In this work, we solve the low-lying eigenpairs of the chiral fermion directly, and then present the result of the spectrum  $\mathcal{D}$  with the smallest statistical uncertainty to date on 2+1 flavor physical quark mass ensembles at two lattice spacings.

*Methodology:* The overlap fermion was proposed in Ref. [17, 18] to construct a discretized fermion action satisfying the Ginsburg-Wilson relation  $D_{ov}\gamma_5 + \gamma_5 D_{ov} = \frac{a}{M_0} D_{ov}\gamma_5 D_{ov}$  [19],

$$D_{ov} = M_0 \left( 1 + \gamma_5 \epsilon(H_w(-M_0)) \right), \quad (1)$$

where  $\epsilon(H_w) = \frac{H_w}{\sqrt{H_w^2}}$  is the matrix sign function,  $H_w(-M_0) = \gamma_5 D_w(-M_0)$  and  $D_w$  is the Wilson Dirac operator with a negative mass parameter such as  $M_0 = 1.5$  to avoid the singularity in  $1/D_w$ .  $\epsilon(H)$  can be decomposed into a combination of the small and large eigenvalue regions,

$$\begin{aligned} \epsilon(H_w) = & \sum_{\lambda_{H,i} < \lambda_H^{\text{cut}}} \frac{\lambda_{H,i}}{|\lambda_{H,i}|} \mathbf{v}_{H,i} (\mathbf{v}_{H,i})^\dagger \\ & + \left( 1 - \sum_{\lambda_{H,i} < \lambda_H^{\text{cut}}} \mathbf{v}_{H,i} (\mathbf{v}_{H,i})^\dagger \right) \sum_i^N d_i H_w^{2i+1}, \quad (2) \end{aligned}$$

in which the eigenpair  $(\lambda_{H,i}, \mathbf{v}_{H,i})$  satisfies the relation  $H_w \mathbf{v}_{H,i} = \lambda_{H,i} \mathbf{v}_{H,i}$ , and  $d_{i=0,1,2,\dots,N}$  are the Chebyshev polynomial coefficients to approximate  $\epsilon(H_w)$  for all the eigenvalues larger than a given cutoff  $\lambda_H^{\text{cut}}$  with a given accuracy [20]. The computational cost of  $D_{ov}$  is proportional to the polynomial order  $N$  and one can increase  $\lambda_H^{\text{cut}}$  to reduce  $N$  until the  $\lambda^H$  become very dense for  $\lambda_H^{\text{cut}} \sim 0.2/a$ . Even for optimal  $\lambda_H^{\text{cut}}$  we still have  $N \sim 100$ ; thus, such a large  $N$  makes the computational cost of  $D_{ov}$  two orders of magnitude higher than that of a  $D_w$ .

The chiral Dirac operator can be defined through  $D_{ov}$ ,

$$D_c = \frac{D_{ov}}{1 - \frac{1}{2M_0} D_{ov}} = \frac{M_0}{2} \frac{1 + \gamma_5 \epsilon(\gamma_5 D_w(M_0))}{1 - \gamma_5 \epsilon(\gamma_5 D_w(M_0))}, \quad (3)$$

and satisfies the same commutation relation  $D_c \gamma_5 + \gamma_5 D_c = 0$  as that of  $\mathcal{D}$  in the continuum. Each eigenvector of  $D_c$  is exactly the same as that of  $D_{ov}$ , and the eigenvalue  $i\lambda_c$  of  $D_c$  can be obtained from that of  $D_{ov}$  with the relation  $i\lambda_c = \frac{\lambda_{ov}}{1 - \frac{1}{2M_0} \lambda_{ov}}$  and is purely imaginary.

Using the Arnoldi factorization algorithm [21], one can obtain the low-lying eigenpairs of  $D_{ov}$ , and thus those of  $D_c$ . Both  $D_{ov}$  and  $D_c$  are similar to  $D_w(0)$  at the continuum limit while providing a proper ultraviolet cutoff to preserve chiral symmetry. Then we can define the eigenvalue density of  $D_c$  as  $\rho(\lambda_c) \equiv \frac{\partial n(\lambda_c)}{V \partial \lambda_c}$ , where  $V = L^3 \times T$  is the 4-D volume and  $n(\lambda_c)$  is the number of eigenvalues in the range  $(0, i\lambda_c]$ . Since  $\rho(\lambda_c)$  is so far the best approximation of the long distance spectrum of a quark on a discretized lattice, we will just treat  $\lambda_c$  as  $\lambda$  in the following discussions.

Based on the partially quenched chiral perturbative theory (PQ $\chi$ PT) which can accommodate the valence quark masses being different from the sea quark masses, one can derive the formula to describe  $\langle \bar{\psi}\psi \rangle$  of the valence quark as a function of both valence and sea quark masses. In PQ $\chi$ PT [2], the density  $\rho(\lambda)$  of the low-lying eigenvalues as the chiral condensate  $\langle \bar{\psi}\psi \rangle$  with virtual quark mass  $i\lambda$  in a finite volume  $V = L^3 \times T$  has the expression,

$$\begin{aligned} \rho(\lambda, V) = & \lim_{\epsilon \rightarrow 0} \frac{1}{2\pi} \left( \langle \bar{\psi}\psi \rangle |_{m_v=i\lambda-\epsilon} - \langle \bar{\psi}\psi \rangle |_{m_v=i\lambda+\epsilon} \right) \\ = & \frac{\Sigma}{\pi} \text{Re} [Z_v(i\lambda, m_q^{sea}) \hat{\Sigma}^{PQ}(i\lambda V, m_q V)], \quad (4) \end{aligned}$$

where  $\Sigma \equiv -\langle \bar{\psi}\psi \rangle |_{m_q \rightarrow 0}$  is the chiral condensate in the chiral limit of  $N_f$  flavors, and  $m_q$  is the light or strange sea quark mass. The standard NLO correction

$$\begin{aligned} Z_v = & 1 + \beta_1(L, T) \frac{N_f^2 - 1}{N_f} \frac{1}{F^2 \sqrt{V}} + \frac{N_f^2 - 4}{N_f} \frac{\lambda \Sigma}{32\pi F^4} \\ & + \mathcal{O}(m_q^{sea}, \lambda^2) \quad (5) \end{aligned}$$

can have leading order finite-volume correction which is  $\sim 4\%$  with  $N_f = 2$  for a  $(5.5 \text{ fm})^4$  lattice [22], and also the  $\lambda$ -dependent finite volume correction,

$$\begin{aligned} \hat{\Sigma}^{PQ}(i\lambda V, m_q V) = & 1 - \frac{1}{\Sigma V} \left( \sum_{q=u,d,s} \frac{1}{i\lambda + m_q} \right. \\ & \left. + \frac{1}{2\lambda^2 \sum_{q=u,d,s} \frac{1}{m_q}} \right) + \mathcal{O}((m_q)^2, \lambda^2, \frac{1}{V^2}), \quad (6) \end{aligned}$$

is suppressed at large  $\lambda$ . It is important to note that  $Z_v$  can differ from 1 by  $\sim 30\%$  or more if we keep the strange quark mass at the physical point, and it makes the  $\Sigma$  in the  $N_f = 2$  and 3 chiral limits quite different from each other. We skip the complete NLO expression of  $\rho(\lambda, V)$  since it is very lengthy, especially in the  $N_f = 2+1$  case, and the interested reader can find it in Ref. [2].

TABLE I. Information of the RBC ensembles [23, 24] used in this calculation. The pion and kaon masses are in unit of MeV.

Symbol	$L^3 \times T$	$a$ (fm)	$m_\pi$	$m_K$	$Z_S$	$ N_{\text{cfg}} $
48I	$48^3 \times 96$	0.1141(2)	139	499	1.135(1)(16)	303
64I	$64^3 \times 128$	0.0837(2)	139	508	1.020(1)(15)	304
48IF	$48^3 \times 96$	0.0711(3)	234	564	0.986(1)(15)	185
32IF	$32^3 \times 64$	0.0626(4)	371	558	0.951(2)(14)	50

*Numerical setup:* We list the four ensembles we used in this work in Table I, which include two ensembles at physical light and strange quark masses. We will use just the first three ensembles to extract  $\rho(\lambda)$ , and the last ensemble with smallest lattice spacing will just be used to show the lattice spacing dependence of the scalar renormalization constant. With one step of HYP smearing [25], we need 800  $H_w$  eigenpairs and 1000 pairs of  $D_c$  eigenpairs to reach the upper bands 0.158 and  $\pm 0.056i$

respectively on the largest 64I ensemble, while the same upper bands can be reached with only  $\sim 180 H_w$  eigenpairs and  $\sim 60$  pairs of  $D_c$  eigenpairs on the  $24^3 \times 64$  ensemble at 0.1105(2) fm.

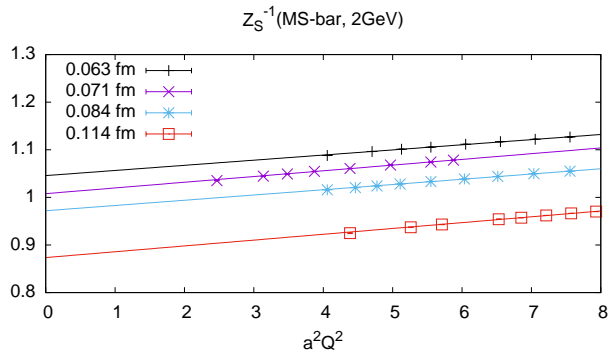


FIG. 1. The inverse of the scalar current renormalization constant at  $\overline{\text{MS}}$  2 GeV and different lattice spacings, as a function of RI/MOM off-shell scale  $Q^2$ . The  $a^2 Q^2$  dependencies in the figure at different lattice spacings are similar, which means that the residual  $Q^2$  dependence vanishes in the continuum limit.

The bare chiral condensate and  $\rho(\lambda)$  we obtained above are under the lattice regularization and require renormalization. To renormalize the scalar quark bi-linear operator, we use the regularization independent momentum subtraction (RI/MOM) scheme [26, 27] under the Landau gauge, and further convert the result into  $\overline{\text{MS}}$  2 GeV as  $\langle \psi\psi \rangle^r = Z_S \langle \bar{\psi}\psi \rangle^b$  and  $\rho(\lambda)^r = Z_m \rho(\lambda)^b = Z_S^{-1} \rho(\lambda)^b$ . The relation  $Z_m Z_S = 1$  is satisfied automatically for the overlap fermion and, crucially, it avoids the systematic uncertainty from the additional chiral symmetry breaking in the Wilson-like actions. In terms of  $Z_S^{-1}$ , the residual RI/MOM scheme  $Q^2$  dependence is proportional to  $a^2$  and will vanish in the continuum limit, since the  $a^2 Q^2$  dependence shown in Fig. 1 is roughly the same at all the lattice spacings we have. The statistical uncertainty in Fig. 1 is at the 0.1% level due to the volume source propagator [28] with a given  $Q^2$ , but the total systematic uncertainties are  $\sim 1.5\%$  which come predominantly from the estimated 4-loop effect in the perturbative matching between RI/MOM and  $\overline{\text{MS}}$  scheme ( $\sim 90\%$  of this 1.5%), and also from the value of  $\Lambda_{QCD}$ , scale running, lattice spacing, and fit range. Fortunately most of the systematic uncertainties are fully correlated at all the lattice spacings and are not enlarged in the continuum extrapolation. Our results of the scalar current renormalization constants are listed in Table I, with two uncertainties from the statistics and systematics. The  $Z_S$  obtained through the alternative symmetric momentum subtraction (RI/SMOM) scheme [29, 30] are consistent with those values above with large systematic uncertainties, as shown in the supplemental materials [31].

*Results:* In Fig. 2, we plot our  $(\pi\rho(\lambda))^{1/3}$  result at 0.084 fm with 0.5, 1, 2, and 4 MeV bin size. The uncer-

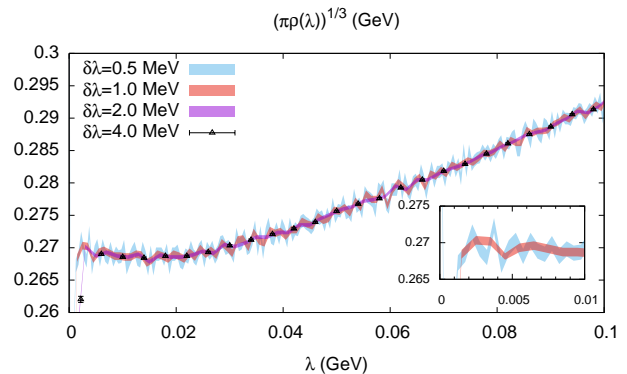


FIG. 2. The  $\lambda$  dependence of  $(\pi\rho(\lambda))^{1/3}$  results at 0.084 fm. Different curves show the results with different bin sizes. The number of eigenvalues in the bin will be smaller than 25 when  $\delta\lambda < 3$  MeV and causes obvious fluctuations, but the data are still flat (up to the statistical fluctuation) when  $\lambda \geq 1$  MeV even with the smallest bin size.

tainty and fluctuation of our results become much larger with smaller bin size since the the number of eigenvalues in each bin is fewer and violates the central limit theorem requirement, but the uncertainty is just 1% with the smallest bin size. With the 0.5 MeV bin size, only the first two data points drop significantly and it suggests that the finite volume effect is relatively small with the 5.5 fm box at the physical pion mass. Based on the standard statistical requirement to have at least 25 samples in each bin ( $\sim 3$  MeV bin size), we choose to use a 5 MeV bin size in the rest of analysis of this work. With such a bin size, our statistical uncertainty is an order of magnitude smaller than those of all the previous  $\rho(\lambda)$  calculations [4, 7–10, 12]. This is understandable since the number of eigenvalues is almost proportional to the physical volume, and we used the largest volume to date in this work.

Next, we show the results at both 0.084 fm and 0.114 fm in Fig. 3. If we ignore the difference between the physical point (the  $u/d$  quark masses are  $m_l \sim 3$  MeV) and chiral limit,  $\pi\rho(\lambda)$  is roughly the chiral condensate  $\Sigma$  at the  $N_f = 2$  chiral limit when  $\lambda \ll m_s$ . As shown in Fig. 3, our results of  $(\pi\rho(\lambda))^{1/3}$  (red and blue bands) with  $\lambda < 50$  MeV are consistent with the present lattice QCD averages  $\Sigma^{1/3} = 272(5)$  MeV [32] (gray band). On the other hand, the results at the two lattice spacings are significantly different ( $\sim 5\%$  on  $\rho(\lambda)$  with  $\lambda \sim 30$  MeV) given their 0.2% uncertainties. The difference of the results at two lattice spacings should be an  $\mathcal{O}(a^2)$  discretization error and is found to be proportional to  $\lambda$  in the range  $\lambda \in (10, 100)$  MeV; thus we subtract a single  $\frac{\lambda \Sigma}{F^2} a^2$  term on the data and obtain the blue and red points in Fig. 3. After the subtraction, we can still see visible differences at  $\rho \sim 7.5$  MeV and 12.5 MeV; this may be due to the residual mixed action effect, but should vanish in the continuum limit. Thus in our further analysis with PQ $\chi$ PT, we always subtract the  $\frac{\lambda \Sigma}{F^2} a^2$  term and drop the

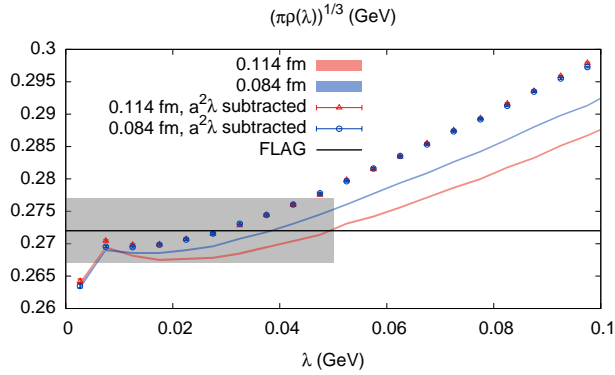


FIG. 3. The  $(\pi\rho(\lambda))^{1/3}$  at 0.084 fm (red band) and 0.114 fm (blue band) with physical light and strange quark masses. By subtracting a single  $\frac{\lambda\Sigma}{F^2}a^2$  term, the data at two lattice spacings (red and blue data points) agree with each other within 1% difference. The gray band shows the present lattice QCD  $N_f = 2$  average of  $\Sigma^{1/3} = (\pi \lim_{m_l \rightarrow 0} \lim_{\lambda \rightarrow 0} \lim_{V \rightarrow \infty} \rho(\lambda))^{1/3}$  [1, 32].

data points with  $\lambda < 13$  MeV.

In order to extract the low energy constant and quark mass information, we present the following three cases:

1. Fix the pion decay constant at the  $N_f = 2$  chiral limit to be its lattice average  $F = 86.2(5)$  MeV [32], treat the light quark mass as a free parameter, and then fit  $\Sigma^{1/3}$  and  $m_l$  at three lattice spacings (0.114, 0.084 and 0.071 fm) in the range  $\lambda \in (12, 30)$  MeV. With a linear  $\mathcal{O}(a^2)$  continuum extrapolation, we estimate  $\Sigma^{1/3}$  and  $m_l$  as  $260.3(0.7)(1.3)(0.7)(0.8)$  MeV and  $4.34(35)(6)(43)(1)$  MeV, respectively, with four uncertainties coming from the statistical fluctuations, renormalization constants, continuum extrapolation (taking the difference between those at the finest lattice spacing and continuum), and the uncertainty of the lattice spacing determination. As illustrated in the top panel of Fig. 4, our value of  $\Sigma$  is consistent with all the Dirac spectrum determinations [9, 10, 12] and has much better control of the statistical and the systematic uncertainties, but is obviously smaller than some of the pion spectrum results [23, 40] with comparable statistical uncertainties. It is worthwhile to mention that the most recent ETMC result (ETM21) [45] is between our result and those from [23, 40].

2. Treat the quark mass  $m_l$ , chiral condensate  $\Sigma_0$  and pion decay constant  $F_0$  in the  $N_f = 3$  chiral limit as free parameters to fit the data in the range  $\lambda \in (15, 100)$  MeV at three lattice spacings separately. The strange quark mass is rewritten into a function of the pion and kaon masses. Our estimate of  $\Sigma_0^{1/3} = 231(8)(1)(1)(1)$  MeV is much more precise compared to all the previous determinations, as shown in Fig. 4. Combined with the value of  $\Sigma$ , we have  $\Sigma/\Sigma_0 = 1.40(2)(2)$  and it reflects the difference between the  $N_f = 2$  chiral limit ( $m_s \sim 90$  MeV) and the  $N_f = 3$  chiral limit ( $m_s = 0$ ), as in the NLO ex-

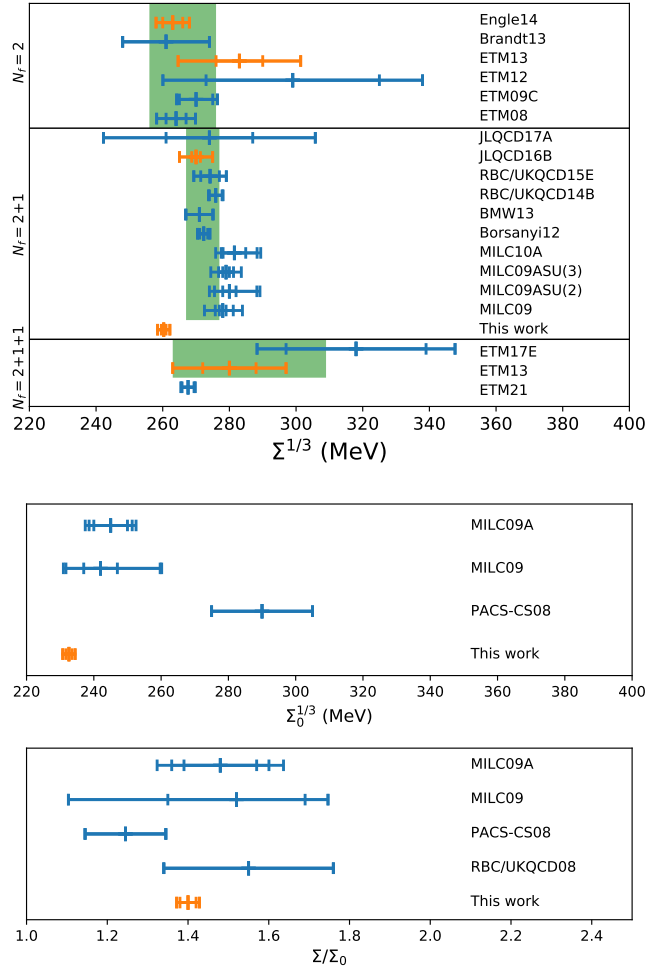


FIG. 4. Results of  $SU(2)$  chiral condensate  $\Sigma^{1/3}$  (upper panel),  $SU(3)$  chiral condensate  $\Sigma_0^{1/3}$  (middle panel) and the ratio of  $\Sigma/\Sigma_0$  (lower panel) from different lattice calculations. Numbers are taken from Refs. [12](Engle14), [33](Brandt13), [34](ETM12), [35](ETM09C), [36](ETM08), [37](JLQCD17A), [9](JLQCD16B), [38](RBC/UKQCD15E), [23](RBC/UKQCD14B), [39](BMW13), [40](Borsanyi12), [41](MILC10A), [42](MILC09ASU(3), MILC09ASU(2)), [43](MILC09), [44](ETM17E), [10](ETM13), [45](ETM21), [46](PACS-CS08), and [47](RBC/UKQCD08). In the upper panel, orange points with error bars are from lattice works using the Dirac spectrum method, while blue ones are from lattice works using other methods. The green bands indicate the corresponding lattice average values from FLAG19 [32]. Points that are not covered by the bands are new lattice results which have not been included in the FLAG average yet.

pression of  $Z_v$ . We also get  $F_0 = 67.8(1.2)(0.1)(2.0)(0.8)$  MeV and  $m_l = 2.95(1)(4)(5)(1)$ . Such a  $m_l$  is  $7\sigma$  (or  $12\%$ ) lower than the value  $3.34(5)$  MeV in Ref. [23], and can be assigned to our systematic uncertainty of missing the NNLO effect in the fit of  $\rho(\lambda)$ .

3. Consider the strange quark mass  $m_s$  as a free parameter also, in addition to  $m_l$ ,  $\Sigma_0$  and  $F_0$ . We obtain

$m_s = 97(24)(13)$  which is in agreement with the FLAG average  $92.0(1.1)$  MeV [32], although it is not precise after the uncertainty is doubled during the continuum extrapolation, and the other quantities agree with the previous determination with fixed  $m_s$ .

The details of the fit strategies, systematic uncertainty estimate and the values before the continuum extrapolation can be found in the supplemental materials [31].

*Summary and outlook:* Based on the precise calculation of the spectral density  $\rho(\lambda)$  of  $\mathcal{D}$  on two lattice spacings with a statistical uncertainty at the 0.2% level, we determine  $\Sigma = (260(1)(2) \text{ MeV})^3$  and  $\Sigma_0 = (233(1)(2) \text{ MeV})^3$  at  $\overline{MS}$  2 GeV; and the pion decay constant in the  $N_f = 3$  chiral limit is  $F_0 = 68(1)(3)$  MeV, where two uncertainties come from the statistics and systematics. Current statistics allow us to obtain a  $\Sigma$  using  $\rho(\lambda)$  with  $\sim 3\%$  total uncertainty which is much lower than the most precise determination using the pion spectrum from RBC [23] which uses the SMOM scheme directly at small  $Q^2$  region, while the value from ETMC [45] using the MOM scheme is in the middle. Note that Ref. [40] uses the FLAG averages of the quark mass and did not calculate  $Z_S$  directly, but most precise quark mass results use the SMOM scheme to suppress the systematic uncertainty from perturbative matching. In the supplementary material, we argue that the MOM scheme should be preferred as being more reliable due to empirical ambiguities in fitting with the SMOM scheme (see also [27,48]). This issue should be considered in future studies, and will also have similar impact on the quark mass determinations as hinted in the ETM work [45].

At the same time, the physical light quark mass  $m_l \sim 3$  MeV can make  $Z_v(\lambda, m_l)$  differ from unity (in the chiral limit) by 10% due to the enhancement of the chiral log. Thus we can use  $\rho(\lambda)$  to determine the light quark mass precisely, up to the systematic uncertainty from NNLO corrections. On the other hand, we observe a clear  $\lambda$

dependence of  $\rho(\lambda)$  in the range of  $\lambda \in (20, 100)$  MeV, and it can be explained by the strange quark mass dependence based on the  $N_f = 2+1$  NLO PQ $\chi$ PT form. It means that the strange quark mass also has a significant impact on  $\rho(\lambda)$ .

## ACKNOWLEDGMENT

We thank the RBC and UKQCD collaborations for providing us their DWF gauge configurations. The calculations were performed using the GWU code [48, 49] through the HIP programming model [50]. This work is partially supported by the Guangdong Major Project of Basic and Applied Basic Research No. 2020B0301030008 and by the Science and Technology Program of Guangzhou No. 2019050001. A. A is supported in part by the U.S. Department of Energy, Office of Science, Office of Nuclear Physics under grant no DE-FG02-95ER40907. Y. B. is supported in part by the National Natural Science Foundation of China (NNSFC) under Grant No. 12075253. T. D and K. L are supported by the U.S. DOE Grant No. DE-SC0013065 and DOE Grant No. DE-AC05-06OR23177 which is within the framework of the TMD Topical Collaboration. Y. Y is also supported by the Strategic Priority Research Program of Chinese Academy of Sciences, Grant No. XDC01040100, XDB34030303, and XDPB15 and also a NSFC-DFG joint grant under grant No. 12061131006 and SCHA 458/22. The numerical calculation has majorly been done on the CAS Xiaodao-1 computing environment, and supported by the Strategic Priority Research Program of Chinese Academy of Sciences, Grant No. XDC01040100, and also by the supercomputing system in the Southern Nuclear Science Computing Center (SNSC).

- 
- [1] T. Banks and A. Casher, Nucl. Phys. B **169**, 103 (1980).
  - [2] P. H. Damgaard and H. Fukaya, JHEP **01**, 052 (2009), arXiv:0812.2797 [hep-lat].
  - [3] L. Del Debbio, L. Giusti, M. Luscher, R. Petronzio, and N. Tantalo, JHEP **02**, 011 (2006), arXiv:hep-lat/0512021 [hep-lat].
  - [4] L. Giusti and M. Luscher, JHEP **03**, 013 (2009), arXiv:0812.3638 [hep-lat].
  - [5] T.-W. Chiu and S. V. Zenkin, Phys. Rev. **D59**, 074501 (1999), arXiv:hep-lat/9806019 [hep-lat].
  - [6] R. C. Brower, H. Neff, and K. Orginos, Comput. Phys. Commun. **220**, 1 (2017), arXiv:1206.5214 [hep-lat].
  - [7] H. Fukaya, S. Aoki, T. Chiu, S. Hashimoto, T. Kaneko, J. Noaki, T. Onogi, and N. Yamada (JLQCD, TWQCD), Phys. Rev. D **83**, 074501 (2011), arXiv:1012.4052 [hep-lat].
  - [8] H. Fukaya, S. Aoki, S. Hashimoto, T. Kaneko, J. Noaki, T. Onogi, and N. Yamada (JLQCD), Phys. Rev. Lett. **104**, 122002 (2010), [Erratum: Phys.Rev.Lett. 105, 159901 (2010)], arXiv:0911.5555 [hep-lat].
  - [9] G. Cossu, H. Fukaya, S. Hashimoto, T. Kaneko, and J.-I. Noaki, PTEP **2016**, 093B06 (2016), arXiv:1607.01099 [hep-lat].
  - [10] K. Cichy, E. Garcia-Ramos, and K. Jansen, JHEP **10**, 175 (2013), arXiv:1303.1954 [hep-lat].
  - [11] G. P. Engel, L. Giusti, S. Lottini, and R. Sommer, Phys. Rev. Lett. **114**, 112001 (2015), arXiv:1406.4987 [hep-ph].
  - [12] G. P. Engel, L. Giusti, S. Lottini, and R. Sommer, Phys. Rev. D **91**, 054505 (2015), arXiv:1411.6386 [hep-lat].
  - [13] A. Li *et al.* ( $\chi$ QCD), Phys. Rev. **D82**, 114501 (2010), arXiv:1005.5424 [hep-lat].
  - [14] Y.-B. Yang, A. Alexandru, T. Draper, M. Gong, and K.-F. Liu, Phys. Rev. **D93**, 034503 (2016), arXiv:1509.04616 [hep-lat].
  - [15] J. Liang, Y.-B. Yang, K.-F. Liu, A. Alexandru, T. Draper, and R. S. Sufian, Phys. Rev. **D96**, 034519 (2017), arXiv:1612.04388 [hep-lat].

- [16] M. Gong *et al.* ( $\chi$ QCD), Phys. Rev. **D88**, 014503 (2013), arXiv:1304.1194 [hep-ph].
- [17] T.-W. Chiu, Phys. Rev. **D60**, 034503 (1999), arXiv:hep-lat/9810052 [hep-lat].
- [18] K.-F. Liu, Int. J. Mod. Phys. **A20**, 7241 (2005), arXiv:hep-lat/0206002 [hep-lat].
- [19] P. H. Ginsparg and K. G. Wilson, Phys. Rev. **D25**, 2649 (1982).
- [20] L. Giusti, C. Hoelbling, M. Luscher, and H. Wittig, Comput. Phys. Commun. **153**, 31 (2003), arXiv:hep-lat/0212012 [hep-lat].
- [21] W. E. Arnoldi, Quart. Appl. Math. **9** (1951).
- [22] P. Hasenfratz and H. Leutwyler, Nucl. Phys. **B343**, 241 (1990).
- [23] T. Blum *et al.* (RBC, UKQCD), Phys. Rev. **D93**, 074505 (2016), arXiv:1411.7017 [hep-lat].
- [24] R. D. Mawhinney (RBC, UKQCD), (2019), arXiv:1912.13150 [hep-lat].
- [25] A. Hasenfratz, R. Hoffmann, and F. Knechtli, *Contents of lattice 2001 proceedings*, Nucl. Phys. Proc. Suppl. **106**, 418 (2002), [418(2001)], arXiv:hep-lat/0110168 [hep-lat].
- [26] G. Martinelli, C. Pittori, C. T. Sachrajda, M. Testa, and A. Vladikas, Nucl. Phys. **B445**, 81 (1995), arXiv:hep-lat/9411010 [hep-lat].
- [27] Y. Bi, H. Cai, Y. Chen, M. Gong, K.-F. Liu, Z. Liu, and Y.-B. Yang, Phys. Rev. **D97**, 094501 (2018), arXiv:1710.08678 [hep-lat].
- [28] J.-W. Chen, T. Ishikawa, L. Jin, H.-W. Lin, Y.-B. Yang, J.-H. Zhang, and Y. Zhao, Phys. Rev. **D97**, 014505 (2018), arXiv:1706.01295 [hep-lat].
- [29] Y. Aoki *et al.*, Phys. Rev. **D78**, 054510 (2008), arXiv:0712.1061 [hep-lat].
- [30] C. Sturm, Y. Aoki, N. H. Christ, T. Izubuchi, C. T. C. Sachrajda, and A. Soni, Phys. Rev. **D80**, 014501 (2009), arXiv:0901.2599 [hep-ph].
- [31] Supplementary materials.
- [32] S. Aoki *et al.* (Flavour Lattice Averaging Group), Eur. Phys. J. **C80**, 113 (2020), arXiv:1902.08191 [hep-lat].
- [33] B. B. Brandt, A. Jüttner, and H. Wittig, JHEP **11**, 034 (2013), arXiv:1306.2916 [hep-lat].
- [34] F. Burger, V. Lubicz, M. Müller-Preussker, S. Simula, and C. Urbach, Phys. Rev. D **87**, 034514 (2013), arXiv:1210.0838 [hep-lat].
- [35] R. Baron *et al.* (ETM), JHEP **08**, 097 (2010), arXiv:0911.5061 [hep-lat].
- [36] R. Frezzotti, V. Lubicz, and S. Simula (ETM), Phys. Rev. D **79**, 074506 (2009), arXiv:0812.4042 [hep-lat].
- [37] S. Aoki, G. Cossu, H. Fukaya, S. Hashimoto, and T. Kaneko (JLQCD), PTEP **2018**, 043B07 (2018), arXiv:1705.10906 [hep-lat].
- [38] P. A. Boyle *et al.*, Phys. Rev. **D93**, 054502 (2016), arXiv:1511.01950 [hep-lat].
- [39] S. Dürr *et al.* (Budapest-Marseille-Wuppertal), Phys. Rev. D **90**, 114504 (2014), arXiv:1310.3626 [hep-lat].
- [40] S. Borsanyi, S. Durr, Z. Fodor, S. Krieg, A. Schafer, E. E. Scholz, and K. K. Szabo, Phys. Rev. D **88**, 014513 (2013), arXiv:1205.0788 [hep-lat].
- [41] A. Bazavov *et al.*, PoS **LATTICE2010**, 083 (2010), arXiv:1011.1792 [hep-lat].
- [42] A. Bazavov *et al.* (MILC), PoS **CD09**, 007 (2009), arXiv:0910.2966 [hep-ph].
- [43] A. Bazavov *et al.* (MILC), Rev. Mod. Phys. **82**, 1349 (2010), arXiv:0903.3598 [hep-lat].
- [44] C. Alexandrou, A. Athenodorou, K. Cichy, M. Constantinou, D. P. Horkel, K. Jansen, G. Koutsou, and C. Larkin, Phys. Rev. D **97**, 074503 (2018), arXiv:1709.06596 [hep-lat].
- [45] C. Alexandrou *et al.*, (2021), arXiv:2104.13408 [hep-lat].
- [46] S. Aoki *et al.* (PACS-CS), Phys. Rev. D **79**, 034503 (2009), arXiv:0807.1661 [hep-lat].
- [47] C. Allton *et al.* (RBC-UKQCD), Phys. Rev. D **78**, 114509 (2008), arXiv:0804.0473 [hep-lat].
- [48] A. Alexandru, C. Pelissier, B. Gamari, and F. Lee, J. Comput. Phys. **231**, 1866 (2012), arXiv:1103.5103 [hep-lat].
- [49] A. Alexandru, M. Lujan, C. Pelissier, B. Gamari, and F. X. Lee, in *Proceedings, 2011 Symposium on Application Accelerators in High-Performance Computing (SAAHPC'11): Knoxville, Tennessee, July 19-20, 2011* (2011) pp. 123–130, arXiv:1106.4964 [hep-lat].
- [50] Y.-J. Bi, Y. Xiao, W.-Y. Guo, M. Gong, P. Sun, S. Xu, and Y.-B. Yang, *Proceedings, 37th International Symposium on Lattice Field Theory (Lattice 2019): Wuhan, China, June 16-22 2019*, PoS **LATTICE2019**, 286 (2020), arXiv:2001.05706 [hep-lat].
- [51] L. Chang, Y.-B. Liu, K. Raya, J. Rodríguez-Quintero, and Y.-B. Yang, (2021), arXiv:2105.06596 [hep-lat].
- [52] A. Bazavov *et al.* (MILC), Phys. Rev. D **87**, 054505 (2013), arXiv:1212.4768 [hep-lat].
- [53] N. Hasan, J. Green, S. Meinel, M. Engelhardt, S. Krieg, J. Negele, A. Pochinsky, and S. Syritsyn, Phys. Rev. D **99**, 114505 (2019), arXiv:1903.06487 [hep-lat].

## SUPPLEMENTAL MATERIALS

### A. MOM and SMOM renormalization

In the main text, we use the RI/MOM [26, 27] scheme to obtain the scalar renormalization constant  $Z_S$ , and the major systematic uncertainty of  $Z_S$  comes from the estimated 4-loop effects in the perturbative matching between the RI/MOM and  $\overline{\text{MS}}$  schemes. It is known that the matching coefficient between the symmetric momentum subtraction (RI/SMOM) scheme and  $\overline{\text{MS}}$  scheme is much closer to 1 up to the 2-loop level [29, 30], so that the related systematic uncertainty can be significantly suppressed. In this section, we argue that there are empirical ambiguities in fitting with the SMOM scheme, and it makes the total systematic uncertainty using the SMOM scheme even larger than in the MOM case.

The  $Z_S$  under the MOM and SMOM schemes are defined by

$$\frac{12Z_q^{\text{RI}}(Q)}{\text{Tr}[\Lambda(p, p, I)]_{p^2=-Q^2}} = \frac{C_0}{m_q^2} + Z_S^{\text{MOM}}(Q) + \mathcal{O}(m_q), \quad (7)$$

$$\frac{12Z_q^{\text{RI}'}(Q)}{\text{Tr}[\Lambda(p_1, p_2, I)]_{p_1^2=p_2^2=q^2=-Q^2}} = Z_S^{\text{SMOM}}(Q^2) + \mathcal{O}(m_q), \quad (8)$$

$$Z_q^{\text{RI}}(Q) = \frac{Z_A}{48} \text{Tr}[\gamma_5 \gamma_\mu \Lambda(p, p, \gamma_\mu \gamma_5)]_{p^2=-Q^2}, \quad (9)$$

$$Z_q^{\text{RI}'}(Q) = \frac{Z_A}{48q^2} \text{Tr}[q_\mu \gamma_5 \not{q} \Lambda(p_1, p_2, \gamma_\mu \gamma_5)]_{p_1^2=p_2^2=q^2=-Q^2}, \quad (10)$$

$$Z_A = \frac{2m_q \langle \bar{\psi} \gamma_5 \psi | \pi \rangle}{m_\pi \langle \bar{\psi} \gamma_5 \gamma_4 \psi | \pi \rangle} \Big|_{m_q \rightarrow 0}, \quad (11)$$

$$\Lambda(p, p', \Gamma) = S^{-1}(p_1) \sum_{x,y} e^{-i(p_1 \cdot x - p_2 \cdot y)} \langle \psi(x) \bar{\psi}(0) \psi(0) \bar{\psi}(y) \rangle S^{-1}(p_2), \quad (12)$$

where  $q = p_1 - p_2$  and  $S(p) = \sum_x e^{-i(p \cdot x)} \langle \psi(x) \bar{\psi}(0) \rangle$ . Note that the quark self energy  $Z_q$  is defined through the axial vector normalization constant  $Z_A$ , not the quark propagator directly. Ref. [51] has shown that  $Z_q(Q) = \frac{1}{12p^2} \text{Tr}[\not{p} S^{-1}(p)]$  defined from the quark propagator has much larger discretization error compared to  $Z_q^{\text{RI}'}$  defined in Eq. (10).

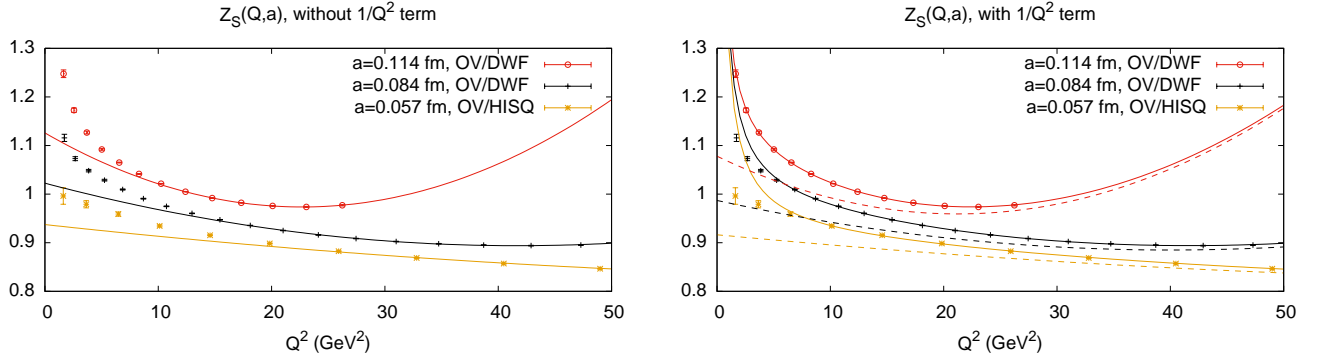


FIG. 5. The scalar renormalization constant  $Z_S$  at  $\overline{\text{MS}}$  2 GeV at three lattice spacings versus the SMOM scale  $Q^2$ . The lattice spacing dependence at  $Q^2 > 20 \text{ GeV}^2$  becomes larger with larger  $Q$ , implying an  $a^2 Q^2$  discretization error. The solid curves in the left panel show the fits using the polynomial form, and those in the right panel use fits with an additional  $1/Q^2$  term to describe the small- $Q^2$  behavior. The dashed curves show the  $Q^2$  dependence with the  $1/Q^2$  term subtracted.

After the corresponding 2-loop matching between the SMOM and  $\overline{\text{MS}}$  schemes, we obtain the  $Z_S$  at  $\overline{\text{MS}}$  2 GeV using different SMOM scale  $Q$ , as shown in Fig. 5. Besides the physical point ensembles we used in the  $\rho(\lambda)$  calculations, we also use the calculation using the overlap fermion on the MILC ensemble [52] with the HISQ sea pion mass 310 MeV at 0.057 fm to show the lattice spacing dependence. As seen in Fig. 5, it is hard to find any linear region where the  $a^2 Q^2$  extrapolation can be made reliably as in the MOM case, as we found on the 48I ensemble with  $a=0.114$  fm

TABLE II. The parameters we obtained from two kinds of the fits with or without the  $c_{-1}^{\text{SMOM}}/Q^2$  term. The lattice spacing dependence of the discretization error coefficients  $c_{1,2}$  are mild.

$a$ (fm)	$ Q_{\min} $ (GeV)	$c_{-1}^{\text{SMOM}}$ (GeV <sup>2</sup> )	$Z_S$	$c_1^{\text{SMOM}}$	$c_2^{\text{SMOM}}$
0.114 fm	3.2	–	1.126(2)	-0.040(1)	0.0026(1)
	1.2	0.32(1)	1.078(3)	-0.033(1)	0.0024(1)
0.084 fm	4.1	–	1.023(2)	-0.034(1)	0.0023(1)
	2.0	0.37(2)	0.987(3)	-0.028(1)	0.0020(1)
0.057 fm	4.9	–	0.937(3)	-0.030(1)	0.0020(1)
	2.2	0.40(3)	0.916(4)	-0.026(1)	0.0018(1)

in the previous study [27]. At the same time, the  $Q^2$  dependence below  $Q^2 < 20$  GeV<sup>2</sup> is also non-linear. Thus we consider the following two empirical forms [27, 53],

$$Z_S^{\text{SMOM,a}}(Q^2) = Z_S + c_1^{\text{SMOM}} a^2 Q^2 + c_2^{\text{SMOM}} a^4 Q^4, \quad (13)$$

$$Z_S^{\text{SMOM,b}}(Q^2) = \frac{c_{-1}^{\text{SMOM}}}{Q^2} + Z_S + c_1^{\text{SMOM}} a^2 Q^2 + c_2^{\text{SMOM}} a^4 Q^4, \quad (14)$$

and tune the minimum  $Q^2$  used in each fit to make  $\chi^2/\text{d.o.f.}$  smaller than 1. The results we obtained are summarized in Table II and illustrated in Fig. 5. We can see that generally the form with the  $1/Q^2$  term can have a better description of the data at small  $Q^2$ , but the  $c_{1,2}^{\text{SMOM}}$  from two fits at different lattice spacings are close to each other. At the same time, the coefficient  $c_{-1}^{\text{SMOM}}$  doesn't vanish in the continuum limit, even though the non-linear behavior at small  $Q^2$  seems to be milder at smaller lattice spacing. The difference of  $Z_S$  from the two fits at three lattice spacings are 0.048(2), 0.036(2) and 0.021(2) respectively, which decreases with  $a$  and thus is likely to be an additional discretization error. Thus we will take the  $Z_S$  from the polynomial fit as the central value and the difference of  $Z_S$  from two fits as a systematic uncertainty.

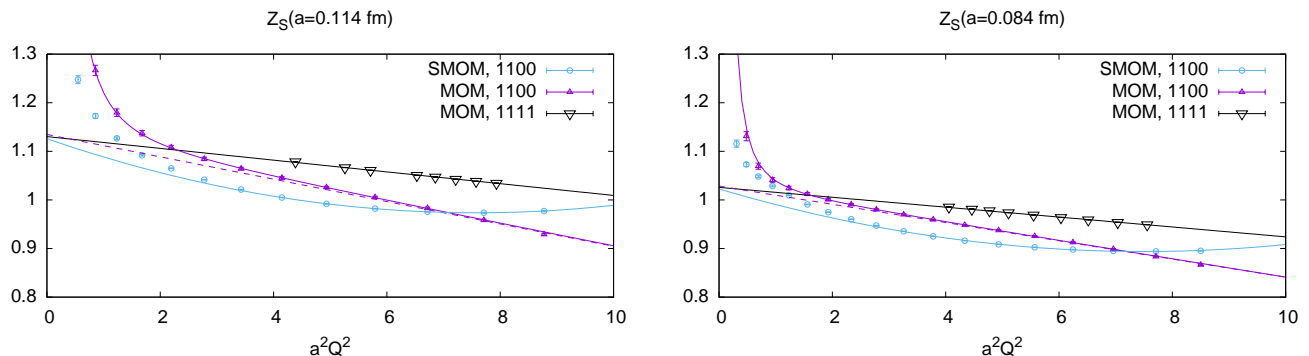


FIG. 6. The scalar renormalization constant  $Z_S$  at  $\overline{\text{MS}}$  2 GeV and two lattice spacings, using two kinds of regularization independent schemes. That using the SMOM scheme with momenta  $p = (k, k, 0, 0)$  and  $p' = (k, 0, k, 0)$  (blue dots) has much larger discretization error than those with the MOM scheme using either  $p = (k, k, 0, 0)$  (purple triangles) or the body-diagonal momenta (black triangles), and the non-perturbative effects exist in both the SMOM and MOM cases at small  $Q^2$ .

Then we can compare the values obtained using the SMOM scheme with those using the MOM scheme. As seen in Fig. 6, the extrapolated values using the SMOM scheme (the intercepts of the blue curves),  $Z_S(a = 0.114\text{fm}) = 1.126(5)(48)$  and  $Z_S(a = 0.084\text{fm}) = 1.023(3)(36)$  at  $\overline{\text{MS}}$  2 GeV, are consistent with the values  $Z_S(a = 0.114\text{fm}) = 1.135(1)(16)$  and  $Z_S(a = 0.084\text{fm}) = 1.020(1)(15)$  using the MOM scheme with the body-diagonal momenta (the intercepts of the black lines) and 3-loop matching. We also calculated the  $Z_S$  using the MOM scheme but with momenta  $p = (k, k, 0, 0)$  with different  $k$  (purple triangles). With an empirical form  $Z^{\text{MOM}}(Q^2) = \frac{C_0^{\text{MOM}}}{Q^4} + Z_0 + C_1^{\text{MOM}} a^2 Q^2$ , which can describe the data in the entire range  $a^2 Q^2 \in [0.5, 9.0]$  with  $\chi^2/\text{d.o.f.} \sim 1$ , the extrapolated values (the intercepts of the purple dashed curves which correspond to the  $Q^2$  dependence with the  $1/Q^4$  term subtracted) are also consistent with those from the other two cases.

Thus even though the perturbative convergence of the matching coefficient between the SMOM and  $\overline{\text{MS}}$  schemes is much better than the MOM case up to 2-loop level, the  $a^2 Q^2$  extrapolation with non-linear  $Q^2$  terms can be quite



TABLE III. Summary of the low energy constants and light quark masses obtained from the fit using the finite volume NLO PQ $\chi$ PT forms in Ref. [2]. All the values are in unit of MeV.

Lattice spacing	$N_f=2$		$N_f=2+1$			$N_f=2+1$ , fit $m_s$			
	$\Sigma^{1/3}$	$m_l$	$\Sigma_0^{1/3}$	$F_0$	$m_l$	$\Sigma_0^{1/3}$	$F_0$	$m_l$	$m_s$
0.114 fm	261.7(0.2)	5.14(15)	229.6(0.3)	62.3(0.4)	3.030(05)	231(1)	64(1)	3.08(07)	74(04)
0.084 fm	261.0(0.3)	4.77(15)	230.9(0.3)	64.7(0.6)	2.993(06)	231(4)	65(4)	3.00(17)	84(12)
0.071 fm	260.5(0.7)		230.5(0.8)	65.8(1.0)					
Continuum	260(1)(2)	4.3(4)(4)	233(1)(2)	68(1)(2)	2.95(1)(36)	231(8)(2)	66(8)(2)	2.89(35)(12)	97(24)(13)
FLAG [32]	272(5)	3.36(4)	245–290	66–84	3.36(4)	245–290	66–84	3.36(4)	92.0(1.1)

sensitive to the empirical form and thus introduces additional systematic uncertainty. If one trivially assumes a good perturbative matching convergence, then uses the value at  $Q = 2$  GeV directly or does the linear  $a^2Q^2$  extrapolation at small  $a^2Q^2$ , then the  $Z_S$  and also  $\Sigma$  can be 5–10% larger. It is also reported in Ref. [53] that using the MOM or SMOM scheme can introduce a systematic uncertainty on the scalar current at the 10% level for the clover fermion.

### B. Fit strategy using the $N_f = 2$ and $N_f = 2 + 1$ PQ $\chi$ PT

We start from the  $N_f = 2+1$  PQ $\chi$ PT, which takes the strange quark into account. With the light and strange quark masses obtained in Ref. [23] and the NLO formula provided in Ref. [2], the  $\chi^2/\text{d.o.f.}$  is generally large regardless of the range of  $\lambda$  we use. Since the NLO correction between the light quark mass and pion mass is  $\sim 10\%$  which is much larger than the statistical uncertainty of the quark mass itself, we treat the quark mass  $m_l$ , chiral condensate  $\Sigma_0$  and pion decay constant  $F_0$  in the  $N_f = 3$  chiral limit as free parameters, to fit the data in the range  $\lambda \in (15, 100)$  MeV at three lattice spacings separately (just the larger two lattice spacings for  $m_l$ ), and extrapolate them to the continuum limit with linear  $\mathcal{O}(a^2)$  correction. The results are listed in Table III. The strange quark mass is still treated as an input using the values determined in Ref. [23]. Our estimate of  $\Sigma_0^{1/3}$ ,  $F_0$  and  $m_l$  are 232.6(0.9)(1.2)(0.7)(0.7) MeV, 67.8(1.2)(0.1)(3.1)(0.8) MeV and 2.945(13)(44)(48)(8) MeV respectively, with four uncertainties coming from the statistical fluctuations, renormalization constants, continuum extrapolation (taking the difference between those at the finest lattice spacing and continuum), and the uncertainty of the lattice spacing determination. Note that the systematic uncertainty of  $F_0$  from the renormalization constant is small as it just depends on the accurate  $Z_A$  but not on the inaccurate  $Z_S$ . Comparing to the previous determinations of  $\Sigma_0^{1/3}$  and  $F_0$ , our determinations are much more precise. On the other hand, the value we obtain for  $m_l$  is  $7\sigma$  (or 12%) lower than the value 3.34(5) MeV in Ref. [23], which explains why our attempts to fit the data with that quark mass result in a large  $\chi^2$ . Thus the NNLO effect in the  $\rho(\lambda)$  expression could be essential to obtain the light quark mass accurately, and we should take this 12% as a systematic uncertainty in our determination of  $m_l$ .

An interesting alternative is to treat the strange quark mass as a free parameter, in order to check what the data can tell us in this case. For this choice, we obtain  $\Sigma_0^{1/3}$ ,  $F_0$ ,  $m_l$  and  $m_s$  as 231(8)(1)(1)(1) MeV, 66(8)(0)(1)(1) MeV, 2.89(35)(5)(11)(1) MeV and 97(24)(1)(13)(0), respectively. The value of  $m_s$  is in agreement with the lattice average 92.0(1.1) MeV, although it is not precise after the uncertainty is doubled during the continuum extrapolation, and the other quantities agree with the previous determination with fixed  $m_s$ , but the uncertainties are much larger.

For comparison, we also consider the  $N_f = 2$  PQ $\chi$ PT case, which assumes the strange quark mass to be much heavier than  $\lambda$  and is thus decoupled from the analysis. As shown in Eq. (5),  $\rho(\lambda)$  is independent of  $\lambda$  with  $N_f = 2$  in the leading order up to the finite volume correction, but a linear  $\lambda$  dependence appears in the  $N_f = 3$  case. The  $N_f = 2$  form is consistent with what we see in Fig. 3 and the  $N_f = 2$  approximation only works when  $\lambda$  is much smaller than the strange quark mass. Since the available  $\lambda$  range is much smaller and we don't know the exact range we should use, we have to fix either the pion decay constant  $F$  in the  $N_f = 2$  chiral limit or the light quark mass  $m_l$  in the fitting. With the light quark mass 3.34(5) MeV obtained in Ref. [23] and the NLO formula provided in Ref. [2], we get the  $N_f = 2$  chiral limit  $\Sigma^{1/3} \sim 265$  MeV and  $F \sim 120$  MeV with  $\chi^2/\text{d.o.f.} \sim 10$  or more in the range  $\lambda \in (15, 40)$  MeV, and  $F$  will be even larger if we reduce the maximum  $\lambda$  used in the fit. In contrast, if we use the lattice QCD average  $F = 86.2(5)$  MeV [32], determined accurately from the chiral extrapolation of the pion decay constant, and treat the light quark mass as a free parameter, we get much better fits to the data at three lattice spacings in the range  $\lambda \in (13, 30)$  MeV with  $\chi^2/\text{d.o.f.}$  around 1. (We reduce the bin size to 3 MeV in order to have 6 data points per bin.) Then we fit the  $\Sigma^{1/3}$  and  $m_l$  at three lattice spacings separately and extrapolate  $\Sigma^{1/3}$  to the continuum with linear  $\mathcal{O}(a^2)$  correction (and also  $m_l$  with two physical pion mass ensembles), as listed in Table III. Our estimates of  $\Sigma^{1/3}$  and  $m_l$  are 260.3(0.7)(1.3)(0.7)(0.8) MeV and 4.34(35)(6)(43)(1) MeV, respectively. It is understandable that the quark mass we obtained can be 30(14)% larger than the lattice QCD averages 3.36(4) MeV due to the NNLO

effect, as we discussed in the  $N_f = 2 + 1$  case.

